Coupling the High Complexity Land Surface Model ACASA to the Mesoscale Model WRF

Liyi Xu, Rex Dave Pyles, Kyaw Tha Paw U,
Shu-Hua Chen and Erwan Monier

MIT JOINT PROGRAM ON THE SCIENCE AND POLICY of GLOBAL CHANGE

Report No. 265
August 2014

The MIT Joint Program on the Science and Policy of Global Change combines cutting-edge scientific research with independent policy analysis to provide a solid foundation for the public and private decisions needed to mitigate and adapt to unavoidable global environmental changes. Being data-driven, the Program uses extensive Earth system and economic data and models to produce quantitative analysis and predictions of the risks of climate change and the challenges of limiting human influence on the environment—essential knowledge for the international dialogue toward a global response to climate change.

To this end, the Program brings together an interdisciplinary group from two established MIT research centers: the Center for Global Change Science (CGCS) and the Center for Energy and Environmental Policy Research (CEEPR). These two centers—along with collaborators from the Marine Biology Laboratory (MBL) at Woods Hole and short- and long-term visitors—provide the united vision needed to solve global challenges.

At the heart of much of the Program's work lies MIT's Integrated Global System Model. Through this integrated model, the Program seeks to: discover new interactions among natural and human climate system components; objectively assess uncertainty in economic and climate projections; critically and quantitatively analyze environmental management and policy proposals; understand complex connections among the many forces that will shape our future; and improve methods to model, monitor and verify greenhouse gas emissions and climatic impacts.

This reprint is one of a series intended to communicate research results and improve public understanding of global environment and energy challenges, thereby contributing to informed debate about climate change and the economic and social implications of policy alternatives.

Ronald G. Prinn and John M. Reilly,
Program Co-Directors

For more information, contact the Program office:
MIT Joint Program on the Science and Policy of Global Change

Postal Address:
Massachusetts Institute of Technology
77 Massachusetts Avenue, E19-411
Cambridge, MA 02139 (USA)

Location:
Building E19, Room 411
400 Main Street, Cambridge

Access:
Tel: (617) 253-7492
Fax: (617) 253-9845
Email: ***globalchange@mit.edu***
Website: ***http://globalchange.mit.edu/***

Coupling the High Complexity Land Surface Model ACASA to the Mesoscale Model WRF

Liyi Xu*†, Rex Dave Pyles‡, Kyaw Tha Paw U‡, Shu-Hua Chen‡ and Erwan Monier*

Abstract

In this study, the Weather Research and Forecasting Model (WRF) is coupled with the Advanced Canopy-Atmosphere-Soil Algorithm (ACASA), a high complexity land surface model. Although WRF is a state-of-the-art regional atmospheric model with high spatial and temporal resolutions, the land surface schemes available in WRF are simple and lack the capability to simulate carbon dioxide (for example, the popular NOAH LSM). ACASA is a complex multilayer land surface model with interactive canopy physiology and full surface hydrological processes. It allows microenvironmental variables such as air and surface temperatures, wind speed, humidity, and carbon dioxide concentration to vary vertically.

Simulations of surface conditions such as air temperature, dew point temperature, and relative humidity from WRF-ACASA and WRF-NOAH are compared with surface observation from over 700 meteorological stations in California. Results show that the increase in complexity in the WRF-ACASA model not only maintains model accuracy, it also properly accounts for the dominant biological and physical processes describing ecosystem-atmosphere interactions that are scientifically valuable. The different complexities of physical and physiological processes in the WRF-ACASA and WRF-NOAH models also highlight the impacts of various land surface and model components on atmospheric and surface conditions.

Contents

1. INTRODUCTION

Although the earth is mostly covered by ocean, the presence of land surfaces introduces much complexity into the earth system that drives numerous atmospheric and oceanic dynamics. The effects of complexity ranges from the simple land-sea contrasts in radiation processes, to the wind flow dynamics, and to the more complex biogeophysical processes of terrestrial systems. Various types of plants, soils, and microbes, as well as all living organisms including humans are situated on and within the landscape that make up the earth's terrestrial system of the biosphere. Though the surface layer represents a very small fraction of the planet—only the lowest

*Joint Program of the Science and Policy on Global Change, Massachusetts Institute of Technology, Cambridge, MA.

†Corresponding author (Email: liyixm@mit.edu)

‡Department of Land, Air, and Water Resources, University of California Davis, Davis, California, USA

10% of the planetary boundary layer—it has been widely regarded as a crucial component of the climate system (Stull, 1988; Mintz, 1981; Rowntree, 1991). The interaction between the land surface (biosphere) and the atmosphere is therefore one of the most active and important aspects of the natural system.

Vegetation at the land surface introduces complex structures, properties, and interactions to the surface layer. Vegetation heavily modifies surface exchanges of energy, gas, moisture and momentum, developing the microenvironment in ways that distinguishing vegetated surfaces from landscapes without vegetation. Such influences are known to occur on different spatial and temporal scales (Chen and Avissar, 1994; Pielke *et al.*, 2002; Zhao *et al.*, 2001). In particular, often near-geostrophically-balanced wind patterns are disrupted in the lower atmosphere when wind encounters vegetated surfaces, i.e., the winds slow down and change direction as a result of turbulent flows that develop within and near the vegetated canopies (Wieringa, 1986; Pyles *et al.*, 2004).

Depending in part on the canopy height and structure, wind and turbulent flows vary considerably across different ecosystems—even when each is presented with the same meteorological and astronomical conditions aloft. Gradients in heating, air pressure, and other forcings develop across heterogeneous landscapes, helping to sustain atmospheric motion. Since the surface layer is the only physical boundary in an atmospheric model, there is a consensus that accurate simulations of atmosphere processes in an atmospheric model require detailed representations of the surface layer and its terrestrial system. Models that account for the effects of surface layer on climate and atmosphere conditions are referred to as Land Surface Models (LSMs).

Unfortunately, the current land surface models, i.e., the widely used set of four schemes present in the Weather Research and Forecasting (WRF) model (5-layer thermal diffusion, Pleim-Xiu, Rapid Update Cycle, and the popular NOAH), often overly simplify the surface layer by using a single layer "big leaf" parameterization and other assumptions, usually based around some form of bulk Monin-Obukhov-type similarity theory (Chen and Dudhia, 2001a,b; Pleim and Xiu, 1995; Smirnova *et al.*, 1997, 2000; Xiu and Pleim, 2001). These models scale the leaf-level physical and physiological properties as one extensive "big leaf" to represent the entire canopy.

The majority of the LSMs do not simulate carbon dioxide flux, even though it is largely recognized as a major contributor to the current climate change phenomenon and a controller of plant physiology. Plant transpiration in these models is often based on the Jarvis parameterization, in which the stomatal control of transpiration is a multiplicative function of meteorological variables such as temperature, humidity, and radiation (Jarvis, 1976). However, a large number of studies show that there is a strong linkage between the physiological process of photosynthetic uptake and the respiratory release of CO_2 to plant transpiration through stomata (Zhan and Kustas, 2001; Houborg and Soegaard, 2004). As such, physiological processes related to CO_2 exchange rates should be included in surface-layer representation of water and energy exchanges.

Oversimplification of surface processes and their impacts on the atmosphere in these land surface models will likely cause the models to misrepresent and poorly predict surface–atmosphere interactions. Models in earth science fields that use simplified equations and statistical relationships to represent complex processes in physics, physiology, hydrology, and thermodynamics

require intense fine-tuning and optimization algorithms for their results to match observations (Duan *et al.*, 1992). These empirical models are capable of producing results that are accurate to a certain extent, but their assumptions limit their ability to investigate relationships and feedback between different components of the system. For example, the empirical models are unable to characterize the relationship between canopy height and sub-canopy energy distribution, and the effects of increased carbon dioxide concentrations on vegetation-atmosphere interactions. This is especially true for regional scale studies, where the influence of the terrestrial system increases with better spatial resolution and heterogeneous land cover.

Recent computer and model developments have greatly improved atmospheric modeling abilities, as progressively more complex planetary boundary layer and surface schemes with higher spatial and temporal resolutions are being implemented. However, the challenges involved in advancing the robustness of land surface models continue to limit the realistic simulation of planetary boundary layer forcings from vegetation, topography, and soil. Some have argued that the increase in model complexity does not translate into higher accuracy due to the increase in uncertainty introduced by the large number of input parameters needed by the more process-based models (Raupach and Finnigan, 1988; Jetten *et al.*, 1999; de Wit, 1999; Perrin *et al.*, 2001). However, there is a certain scientific value in properly accounting for the dominant biological and physical processes describing ecosystem-atmosphere interactions—even if this greatly complicates the models.

This study introduces the novel coupling of the mesoscale WRF model with the complex multilayer Advanced Canopy-Atmosphere-Soil Algorithm (ACASA) model, to improve the surface and atmospheric representation in a regional context. The objectives of this study are to (1) parameterize complex land surface processes that drive local mesoscale circulations, and (2) to investigate the effects of model complexity on accuracy.

2. MODELS, METHODOLOGY AND DATA

2.1 The Weather Research and Forecasting (WRF) Model

The mesoscale model used in this study is the Advanced Research WRF (ARW) model Version 3.1. WRF is a state-of-the-art, mesoscale numerical weather prediction and atmospheric research model developed by a collaborative effort of the National Center for Atmospheric Research (NCAR), the National Oceanic and Atmospheric Administration (NOAA), the Earth System Research Laboratory (ESRL), and other agencies. The WRF model contains a nearly complete set of compressible and non-hydrostatic equations for atmospheric physics (Chen and Dudhia, 2000) to simulate three-dimensional atmospheric variables, and its vertical grid spacing varies in height with smaller spacing between the lower atmospheric layers than the upper atmospheric layers. The mass-based terrain following coordinate in WRF improves the surface processes. It is commonly used to study air quality, precipitation, severe windstorm events, weather forecasts, and other atmospheric conditions (Borge *et al.*, 2008; Thompson *et al.*, 2004; Powers, 2007; Miglietta and Rotunno, 2005; Trenberth and Shea, 2006). Compared to the 2.5° (equivalent to 250 km at the equator) resolution of General Circulation Models (GCMs), the WRF model with high spatial and temporal resolution is better suited for studying climate conditions over

California; WRF can be nested so that finer grid spacing (1 km or less) is possible.

As mentioned in the introduction, four different parameterizations of land-surface processes are available in the WRF model. WRF's more widely used and most sophisticated NOAH employs simplistic physics compared to ACASA, being more akin to the set of ecophysiological schemes that include SiB and BATS (Dickinson *et al.*, 1993; Sellers *et al.*, 1996). There is only one vegetated surface layer in the NOAH scheme, along with four soil layers to calculate soil temperature and moisture. The "big leaf" approach assumes the entire canopy has similar physical and physiological properties to a single big leaf. In addition, energy and mass transfers for the surface layer are calculated using simple surface physics (Noilhan and Planton, 1989; Holtslag and Ek, 1996; Chen and Dudhia, 2000). For example, the surface skin temperature is linearly extrapolated from a single surface energy balance equation, which represents the combined surface layer of ground and vegetation (Mahrt and Ek, 1984). Surface evaporation is computed using modified diurnally dependent Penman-Monteith equation from Mahrt and Ek (1984) and the Jarvis parameterization (Jarvis, 1976). The current WRF LSMs are relatively simple, when compared to the higher order closure based ACASA model, and none of them calculate carbon flux. In contrast, the fully coupled WRF-ACASA model is capable of calculating carbon dioxide fluxes as well as the reaction of the ecosystems to increases in carbon dioxide concentrations.

2.2 The Advanced Canopy-Atmosphere-Soil Algorithm (ACASA) Model

Compared to the simple NOAH, the ACASA model version 2.0 is a complex multilayer analytical land surface model, which simulates the microenvironment profiles and turbulent exchange of energy, mass, CO_2 and momentum within and above ecosystems that constitute land surfaces. It represents the interaction between vegetation, soil and the atmosphere based on physical and biological processes described from the scale of leaves (microscale), and horizontal scales on the order of 100 times the ecosystem vegetation height (i.e., hundreds of meters to around 1 km). The surface layer is represented as a column model with multiple vertical layers extending to the lowest planetary boundary. The model has 10 vertical atmospheric layers above-canopy, 10 intra-canopy layers, and 4 soil layers.

For each canopy layer, leaves are oriented in 9 sun-lit angle leaf classes (random spherical orientation) and 1 shaded leaf class in order to more accurately represent radiation transfer and leaf temperatures in a simulated variable array. This array aggregates the exchanges of sensible heat, water vapor, momentum, and carbon dioxide. The values of fluxes at each layer depend on those from all other layers, so the longwave radiative and turbulence transfer equations are iterated until numerical equilibrium is reached. Shortwave radiation fluxes, along with associated arrays (probabilities of transmission, beam extinction coefficients, etc.) are not changed, while the other sets of equations are iterated to numerical convergence.

Plant physiological processes, such as evapotranspiration, photosynthesis and respiration, are calculated for each of the leaf classes and layers, based on the simulated radiation field and the micrometeorological variables calculated in the previous iteration step. The default maximum rate of Rubisco carboxylase activity, which controls plant physiological processes, is provided for each of the standardized vegetation types, although specific values of these parameters can be

entered. Temperature, mean wind speed, carbon dioxide concentration, and specific humidity are calculated explicitly for each layer, using the higher order closure equations (Meyers and Paw U, 1986, 1987; Su *et al.*, 1996).

In addition to accounting for the carbon dioxide flux, a key advanced component of the ACASA model is its higher-order turbulent closure scheme. The parameterizations of the fourth-order terms used to solve the prognostic third-order equations are described by assuming a quasi-Gaussian probability distribution as a function of second-moment terms (Meyers and Paw U, 1987). Compared to lower order closure models, the higher order closure scheme increases model accuracy by improving representations of the turbulent transport of energy, momentum, and water by both small and large eddies. In small-eddy theory or eddy viscosity, energy fluxes move down a local gradient; however, large eddies in the real atmosphere can transport flux against the local gradient. Such counter-gradient flow is a physical property of large eddies associated with long distance transport. For example, mid-afternoon intermittent ejection-sweep eddies cycling deep into a warm forest canopy with snow on the ground, from regions with air temperature values between that of the warm canopy and the cold snow surface, would result in overturning of eddies to transport relative warm air from above and within the canopy to the snow surface below. The local gradient from the canopy to the above-canopy air would incorrectly indicate sensible heat going upwards—instead of the actual heat flow down through the canopy—due to the long turbulence scales of transport. These potentially counter-gradient transports are responsible for much of land surface evaporation, heat, carbon dioxide and momentum fluxes (Denmead and Bradley, 1985; Gao *et al.*, 1989). The ACASA model uses higher order closure transport between multiple layers of the canopy to simulate non-local transport, allowing the simulation of counter-gradient and non-gradient exchange. By comparison, the simple lower order turbulent closure model NOAH has only one surface layer. It is limited to only down-gradient transport and cannot mix within the canopy.

In the ACASA model, both rain and snow forms of precipitation are intercepted by the canopy elements in each layer. Some of the precipitation is retained on the leaf surfaces to modify the microenvironment of the layers for the next time step, depending on the precipitation amount, canopy storage capacity, and vaporization or sublimation rate. The remaining precipitation is distributed to the ground surface, influencing soil moisture and/or surface runoff as calculated by the layered soil model. The soil model physics in ACASA are very similar to the diffusion physics used in NOAH, but ACASA includes enhanced layering of the snowpack for more detailed thermal profiles throughout deep snow. This multilayer snow model allows interactions between layers, and more effectively calculates energy distribution and snow hydrological processes (e.g., snow melt) when surface snow experiences higher or lower temperatures than the underlying snow layers. This is especially relevant over regions with high snow depth such as Sierra Nevada Mountain, where snow is a significant source of water. The multilayer snow hydrology scheme has been well tested during the SNOWMIP project (Etchevers *et al.*, 2004; Rutter *et al.*, 2009), where ACASA performed at least as well as many snow models by accurately estimating the snow accumulation rate as well as the timing of snow melt in a wide range of biomes.

The stand-alone version of the ACASA model has been successfully applied to study sites

across different countries, climate systems, and vegetation types. These include a 500-year old-growth coniferous forest at the Wind River Canopy Crane Research Facility in Washington State (Pyles *et al.*, 2000, 2004), a spruce forest in in the Fichtelgebirge Mountains in Germany (Staudt *et al.*, 2011), a maquis ecosystem in Sardinia near Alghero (Marras *et al.*, 2008), and a grape vineyard in Tuscany near Montelcino, Italy (Marras *et al.*, 2011).

2.3 The WRF-ACASA Coupling

In an effort to improve the parameterization of land surface processes and their feedbacks with the atmosphere, ACASA is coupled to the mesoscale model WRF as a new land surface scheme. The schematic diagram of **Figure 1** represents the coupling between the two models. From the Planetary Boundary Layer (PBL) and above, the WRF model provides meteorological variables as input forcing to the ACASA land surface model at the lowest WRF sigma-layer. These variables include solar shortwave and terrestrial (atmospheric thermal long-wave) radiation, precipitation, humidity, wind speed, carbon dioxide concentration, and barometric pressure. Radiation is partitioned into thermal IR, visible (PAR) and NIR by the ACASA model, which treats these radiation streams separately according to the preferential scattering of the different wavelengths as the radiation passes through the canopy. Part of the radiation is reflected back to the PBL according to the layered canopy radiative transfer model, with the remaining radiation driving the canopy energy balance components and photosynthesis.

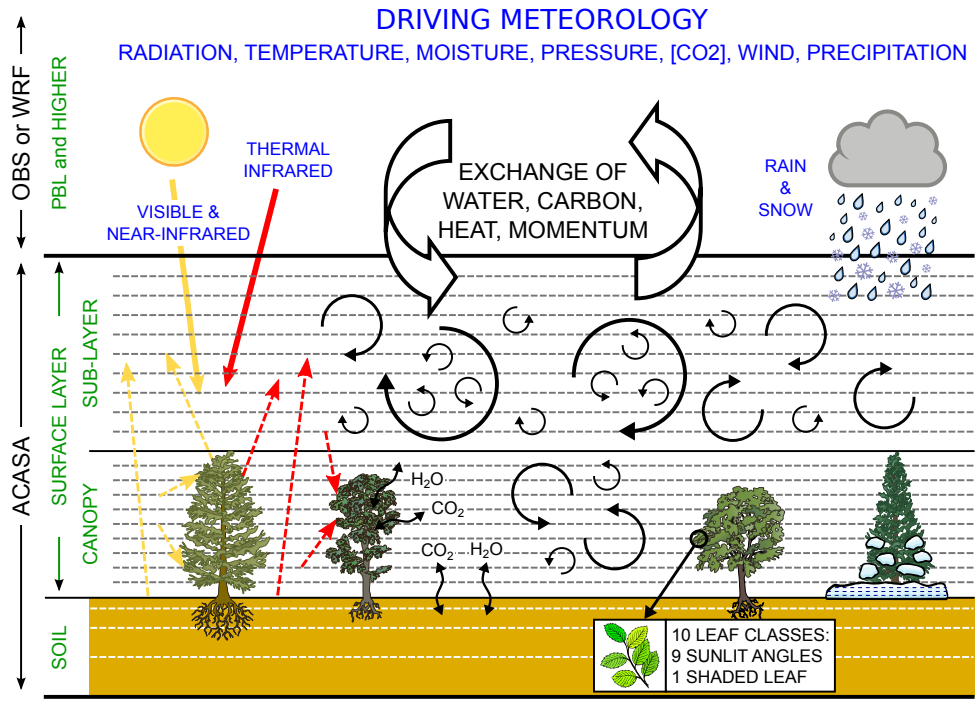

Figure 1. The schematic diagram of the WRF-ACASA coupling.

Unlike the "big leaf" model NOAH, ACASA creates a normalized vertical Leaf Area Index (LAI) or Leaf Area Density (LAD) for the multiple canopy layers according to vegetation type.

This is crucial because the canopy height and distribution of LAD directly influence the interactions of wind, light, temperature, radiation, and carbon between the atmosphere and the surface layer.

2.4 Model Setup

The WRF model requires input data for prognostic variables including wind, temperature, moisture, radiation, and soil temperature, both for an initialized field of variables through the domain, and at the boundaries of the domain. In this study, these input data are provided by the Northern America Regional Reanalysis (NARR) dataset to drive both the WRF-NOAH and WRF-ACASA models. Unlike many other reanalysis data sets with coarse spatial resolution such as ERA40 (European Center for Medium-Range Weather Forecasts 40 Year Re-analysis) and GFS (Global Forecast System), NARR is a regional data set specifically developed for the Northern American region. The temporal and spatial resolutions of this data set are 3 hours and 32 km, respectively.

Simulations of both the default WRF-NOAH and the WRF-ACASA models were performed for two year-long simulations (2005 and 2006) with horizontal grid spacing of 8 km x 8 km. These years were chosen because they provide the most extensive set of surface observation data. The model domain covers all of California with parts of neighboring states and the Pacific Ocean to the west, shown in **Figure 2**. The complex terrain and vast ecological and climatic systems in the region make this domain ideal for testing the WRF-NOAH and WRF-ACASA coupled model performances. The geological and ecological regions extend eastward from the coastal range shrublands to the Central Valley grasslands and croplands, then to the foothill woodlands before finishing at the coniferous forests along the Sierra Nevada range. Areas further inland to the east and south include the Great Basin and Range Chaos, an arid and complex mosaic of forests and chaparral tessellated amid the myriad fossae that erupt between dunes and playas. The contrasting moist Northern and semiarid Southern California landscapes are also represented in tandem.

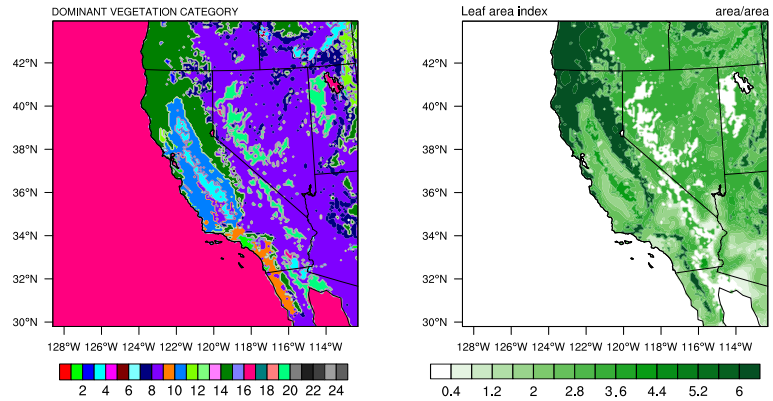

Figure 2. The complex topography and land cover of the study domain is represented here by: (left) Dominant vegetation type and (right) Leaf Area Index (LAI) from USGS used by the WRF model. The horizontal grid spacing of 8 km is needed to resolve the major topographical and ecological features of the domain.

Aside from the differences in the land surface model, both WRF-NOAH and WRF-ACASA

employ the same set of atmosphere physics schemes stemming from the WRF model. These include the Purdue Lin *et al.* scheme for microphysics (Chen and Sun, 2002), the Rapid Radiative Transfer Model for long wave radiation (Mlawer *et al.*, 1997), the Dudhia scheme for shortwave radiation (Dudhia, 1989), the Monin-Obukhov Similarity scheme for surface layer physics of non-vegetated surfaces and the ocean, and the MRF scheme for the planetary boundary layer (Hong and Pan, 1996). WRF runs its atmospheric processes at a 60-second time step, while the radiation scheme and the land surface schemes are called every 30 minutes. Because ACASA assumes quasi-steady-state turbulent processes, its physics are not considered advisable for shorter time intervals. Both NOAH and ACASA calculate surface processes and update the radiation balance, as well as heat flux, water vapor flux, carbon flux, surface temperature, snow water equivalent, and other surface variables in WRF. Analytical nudging of four dimensional data assimilation (FDDA) is applied to the atmosphere for all model simulations in order to maintain the large-scale consistency and reduce drifting of model simulation from the driving field over time. Such nudging (FDDA) is commonly practiced in limited-area modeling, and current methods active in WRF are widely accepted due to rigorous testing (Stauffer and Seaman, 1990; Stauffer *et al.*, 1991).

2.5 Data

The main independent observational datasets used to evaluate the model simulations were obtained from the Meteorological Section of the California Air Resource Board (ARB). The NARR data were not used for the evaluation as the dataset was used for FDDA during both model simulations. The ARB meteorology dataset is compiled from over 2000 surface observation stations in California from multiple agencies and programs: Remote Automated Weather Stations (RAWS) from the National Interagency Fire Center, the California Irrigation Management Information System (CIMIS), National Oceanic and Atmospheric Administration (NOAA), Aerometric Information Retrieval System (AIRS), and the Federal Aviation Administration. Potential measurement errors and uncertainties are expected in the ARB data because of the differences in station setups and measurement standards from the different agencies. For example, ambient surface air temperature is measured at various heights from 1 to 10 meters above the ground, depending on the measuring agency. Some stations are located in urban environments, while the model simulations are structured to study natural vegetated environments. Therefore, some discrepancies between the observation and simulation are likely to occur in densely populated areas. However, with hourly data from over 2000 observation stations within the study domain, the ARB dataset remains valuable. Out of the 2000 surface stations in the overall current ARB database, there were about 730 stations operational during the study period of 2005 and 2006 (**Figure 3**).

The meteorological and surface conditions from the WRF-NOAH and WRF-ACASA model simulations were evaluated using the ARB data both for the regional scale level performance, and for specific stations for more in-depth analysis. This represents is the most rigorous test of ACASA to date, in terms of the sheer number of ACASA point-simulations and the number of ACASA points linked in both space and time. This investigation therefore represents a significant elaboration upon earlier work (Pyles *et al.*, 2003). Meteorological variables such as surface air

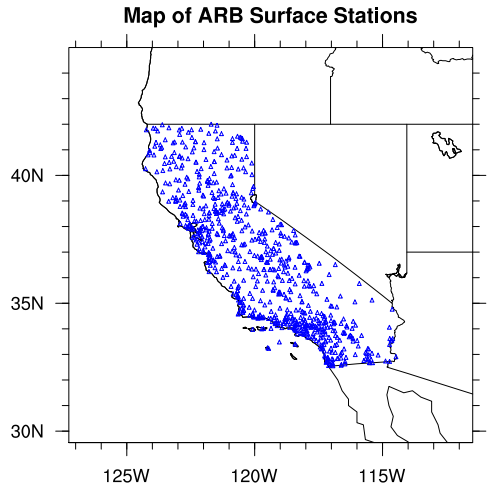

Figure 3. Map of the location of the California Air Resources Board surface stations.

temperature, dew point temperature, and relative humidity from the two model simulations were compared with each other and the observational data. Four basins within the study domain were selected to represent the different vegetation covers and geographic locations within the domain: the Northeast Plateau (NEP) is mostly grassland that covers 32 percent of the landscape; the Mojave Desert (MJ) station located at the southeastern California is mostly shrubland with a 13.75 percent of vegetation cover; the San Joaquin Valley (SJV) is a major agricultural region, covered by irrigated cropland and pasture with about 23 percent of the land covered by vegetation; and the Sierra Nevada Mountain County (MC) with 60 percent of the land covered by high-altitude vegetation (mainly evergreen needle leaf forest). These four basins encompass a total of 240 stations. Measurements from these basins were compared to the WRF-NOAH and WRF-ACASA simulation outputs for the nearest grid points. From each basin, one station was identified for further detail analysis (see **Table 1**).

Table 1. Selected sites from the Air Resources Board meteorological stations network.

Basin	Station ID	Latitude	Longitude	PFT
NEP	5751	41.959	–121.471	Grassland
MD	5780	33.557	–114.666	Shrubland
SJV	5783	35.604	–119.213	Irrigated Cropland and Pasture
MC	5714	38.754	–120.732	Evergreen Needleleaf Forest

Hourly, daily and monthly data were used for model evaluation in this study. Due to the nature of continuous instrument network operations, however, data gaps are inevitable in surface observations. To avoid missing data biases, only the days with complete 24-hour data sets are used for statistical analyses. The reason for this selection of data is illustrated in **Figure 4**. The black line in Figure 4 represents hourly temperature observations for the Mojave Desert Station during June 2006. The red line represents the daily mean temperature only from days with complete 24 hour sets of temperature observation. The black line contains data with missing gaps, which in-

fluence the mean monthly temperature calculation. The monthly mean temperature is lowered if it is calculated using only days with the complete 24 hours rather than all data. This is due to a significant amount of missing data from the daytime that skews the monthly temperature toward the cooler nighttime temperature, resulting in a cold bias. By using only days with complete 24 hours of measurement for statistical analyses, the temperature bias toward any certain period of the day is avoided.

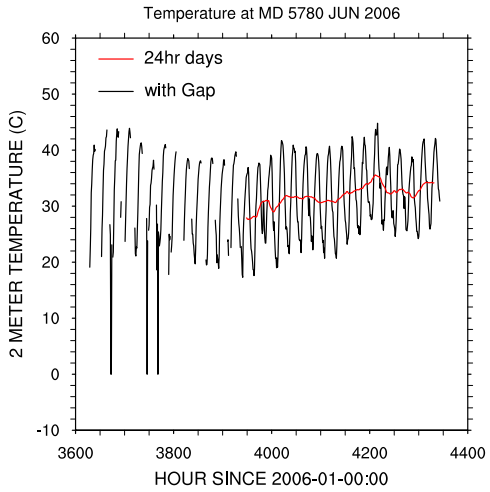

Figure 4. Time series of the surface air temperature at Mojave Desert Station during June 2006. The black line represents the entire set of surface temperature observation with gaps presented. The red line represents the daily mean temperature calculated using only days with all 24 hours of observation available.

Some of the challenges in making a comparison between WRF-ACASA simulations and the observations are that (1) the observation heights were frequently different than the simulated grid point height, and (2) the station landscape type was often different than that of the simulation grid point. Many stations are within patches of specific landscape types that may differ significantly from the overall grid point landscape. Even more challenging is the fact that WRF-ACASA simulations have outputs for the temperatures within a canopy, so for orchards or forests, the 2-meter height (surface) simulation data are not expected to match well with the 2-meter height observations. For the taller plant ecosystems, WRF-ACASA simulations at the 2-meter height represent temperatures within the plant canopy or understory; yet, the observations from the ARB network are never in such locations. Rather, they are over other surfaces not representative of the simulation grid-point—and are usually not even at the 2-meter height. The WRF-NOAH simulations do not suffer as much in terms of the 2-meter simulations; as the NOAH surface model is a big-leaf model, the 2-meter height includes characteristics more similar to that of the observations. Despite these significant shortcomings, to maximize the number of observations, the ARB data were chosen because of the large number of stations throughout the simulation domain. The results from year 2005 and year 2006 are similar, so only year 2006 is presented here.

3. RESULTS AND DISCUSSION

The monthly mean surface temperatures in California from both model simulations are compared against the surface observations in **Figure 5**. The left panel shows the ARB data (gathered at approximately 10 m above the ground); the white areas represent regions with missing observations. The WRF-NOAH and WRF-ACASA simulation outputs are represented in the center and right panels, respectively. The region's geographical complexity is highlighted by the spatial and temporal variations in the surface temperature. The warm summer and cool winter are typical of a Mediterranean-type climate. In addition to the seasonal variation, both WRF-ACASA and WRF-NOAH models are able to capture the distinct characteristics of the warm Central Valley and semiarid region of Southern California. The large, flat Central Valley is dominated by Irrigated Cropland and Pasture, and surrounded by Cropland/Grassland Mosaic. The cold temperatures over the mountain regions are also visible from the surface temperature field. However, there are noticeable differences between the WRF-ACASA and the WRF-NOAH over the Central Valley.

During the month of February, the WRF-ACASA output distinctly features a colder Central Valley surrounded by a slightly warmer region. A similar effect is also visible in the month of November, when WRF-ACASA again depicts a cold bias over the Central Valley. The temperature contrast of this region is mostly due to differences in land cover type, as well as LAI associated with the land cover (Figure 2). These two variables impact plant physiological processes in the WRF-ACASA model such as photosynthesis, respiration, and evapotranspiration. Lower LAI in the area immediately surrounding Central Valley results in less transpiration than in higher LAI Central Valley areas, which has higher partitioning of available energy to latent heat, and less to sensible heat.

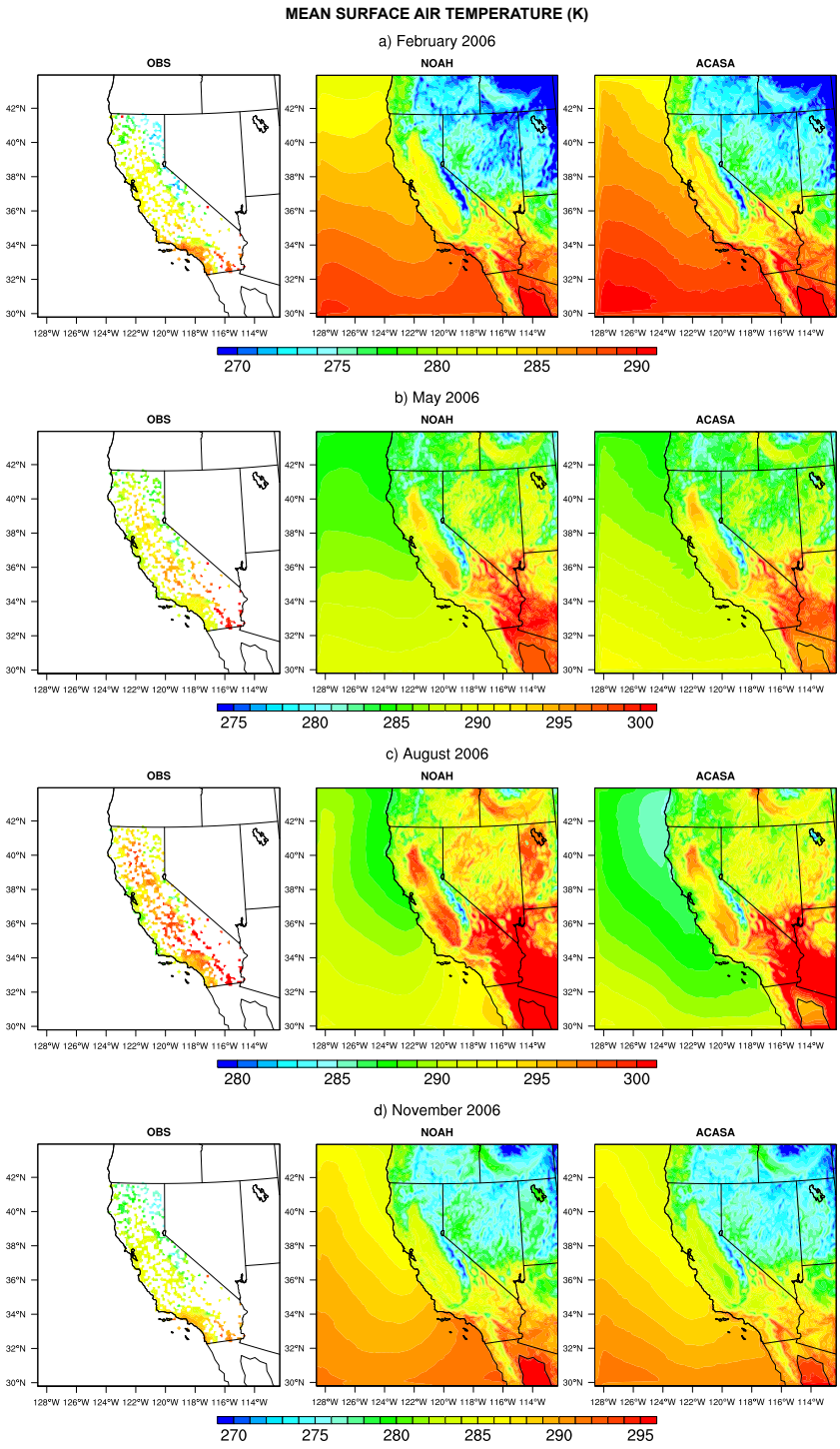

Figure 5. Monthly mean surface air temperature simulated by WRF-ACASA and WRF-NOAH and for the surface observations during the months of February, May, August and November 2006.

While the WRF-ACASA model is highly influenced by vegetation cover and the changes in LAI, the surface processes in WRF-NOAH rely heavily on the prescribed minimum canopy resistance for each vegetation type. Therefore, the contrast in temperature between regions of different vegetation cover and leaf area index is more pronounced in the WRF-ACASA model than the WRF-NOAH model. The overall agreement between the model simulations from WRF-ACASA and WRF-NOAH match well with surface observations throughout the year. However, the WRF-ACASA experiences a cold bias over the high LAI region in the Central Valley during the month of August. Once again, it should be noted that the WRF-ACASA output is generally not at the same height as the observation height, and the actual local vegetation type often differs from that immediately surrounding the observation sites. Close examination in the Central Valley also reveals that the prescribed LAI values in WRF are significantly higher than the remote sensing LAI values during the summer months. Because WRF-ACASA relies on LAI to simulate plant physiological processes and energy budget, this discrepancy in LAI causes WRF-ACASA to overestimate evapotranspiration over the region and to create a cold bias. The WRF-NOAH model is less sensitive in this regard because it uses prescribed canopy resistances. This highlights the conundrum of advancing model physics–more sophisticated models become more susceptible to errors in input data quality as they become more representative of variations in land cover type.

Figure 6 shows a time series of surface air temperature simulated by WRF-ACASA and WRF-NOAH alongside observations from four different stations in 2006 for the months of February, May, August, and November. Both WRF-ACASA and WRF-NOAH perform well in simulating the temporal pattern of temperature changes across the seasons and stations. Even short-term weather events are clearly detectible in the simulated temperature changes. One such example is the Northeast Plateau station during the month of November, when it experienced a 20°C plunge in temperature followed by a warming of 10°C within five days. Both models are able to simulate this short-term weather event.

There are differences between the WRF-ACASA and WRF-NOAH performances in time and location. While the model simulations from both models agree well with the surface observation during the cold months of February and November, they differ during the warmer months. During the month of May over the Mojave Desert station, the WRF-ACASA model started with good agreement with the surface observation, but the difference gradually increased over time, with daily minimums (or nighttime temperatures) becoming cooler than the surface observation. During August, the nighttime temperatures were consistently 3 to 4°C cooler than the observed nighttime temperature. PBL heights at night using both NOAH and ACASA were the same as in minimum sigma-layer heights in WRF. However, this may be excessively shallow given observations suggesting nocturnal PBL heights over deserts to be on the order of 100 to 300 meters (Stull, 1988). ACASA results for nighttime cooling would be subject to a cold bias if the PBL were too shallow, as the negative sensible heat flux would become "trapped" in the shallow inversion layer. ACASA is potentially more sensitive to this than NOAH and related models, due to different minimum turbulent mixing thresholds for Monin-Obukhov similarity vs. higher-order turbulence calculations.

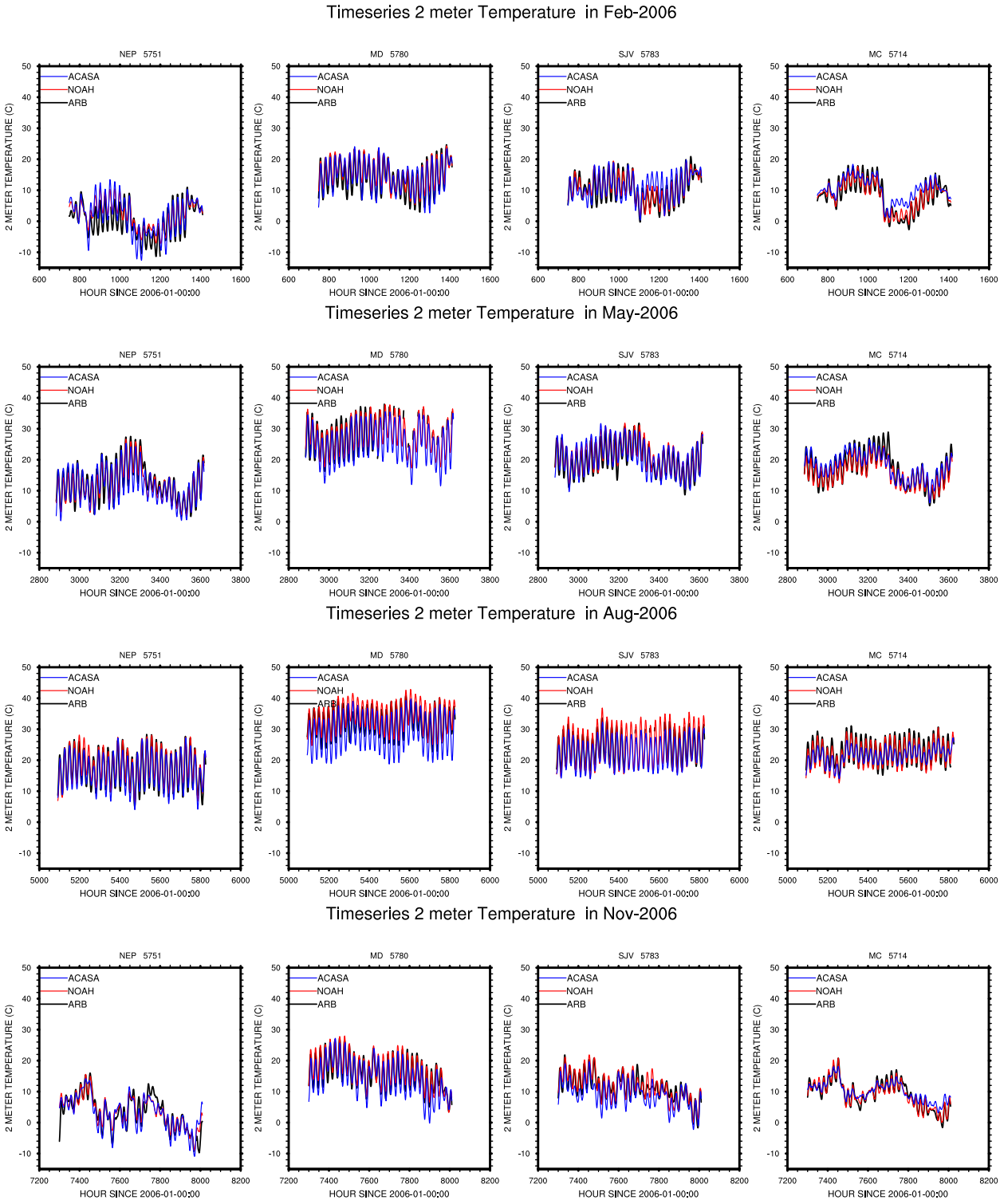

Figure 6. Time series of surface air temperature simulated by WRF-ACASA and WRF-NOAH and for the surface observations for four different stations and during the months of February, May, August and November 2006. From left to right: Northeast Plateau station, Mojave Desert station, San Joaquin Valley station, Mountain County station.

Figure 7 examines differences in the diurnal patterns from each station between the two land surface models over the four seasons. While the simulated diurnal temperatures from the two models fall mostly within the ± 1 standard deviation range from the surface diurnal temperature depending on the season and locations, there are some small differences in times and locations between the two. Both WRF-ACASA and WRF-NOAH perform exceptionally well over the Northeast Plateau station throughout the year, with the WRF-ACASA model performing slightly better than the WRF-NOAH model during the early winter mornings. In summer and (to a lesser extent) autumn over Mojave Desert, the WRF-ACASA model tended to underestimate the temperature during the early mornings. On the other hand, the WRF-NOAH model tended to overestimate summer temperature at 1.0 standard deviations above the mean most of the day. Further investigation shows that the WRF-ACASA morning cooling is likely due to the model's canopy representation. Canopy representation might also be a factor in the slight overestimation of temperature during summer by the WRF-NOAH model. While both WRF-ACASA and WRF-NOAH assign a Shrubland plant functional type to the Mojave Desert site, the WRF-ACASA model also prescribed a 3-meter canopy height to the Shrubland vegetation type. Therefore, the WRF-ACASA model takes longer in the morning to heat up the surface air temperatures of the Mojave Desert site, because it is assumed to be within the canopy. This results in a lag of daytime temperature rise and cooler daily maximum temperatures than the observed values. As the summer ends, however, the diurnal patterns of the WRF-ACASA model once again compare well with the observation, falling within the ± 1 standard deviation range. Not visible in Figure 6, the diurnal patterns of WRF-ACASA over the Mountain County station show that the diurnal variations are smaller than the variations displayed by the surface measurement as well as by the WRF-NOAH simulations. As a result, the WRF-ACASA simulated daytime temperatures during August fall below the observed temperature range. In contrast, the WRF-NOAH model experiences a warm bias during the warmer months of May and August. The daytime temperatures of WRF-NOAH exceed the observed temperature range over San Joaquin Valley station.

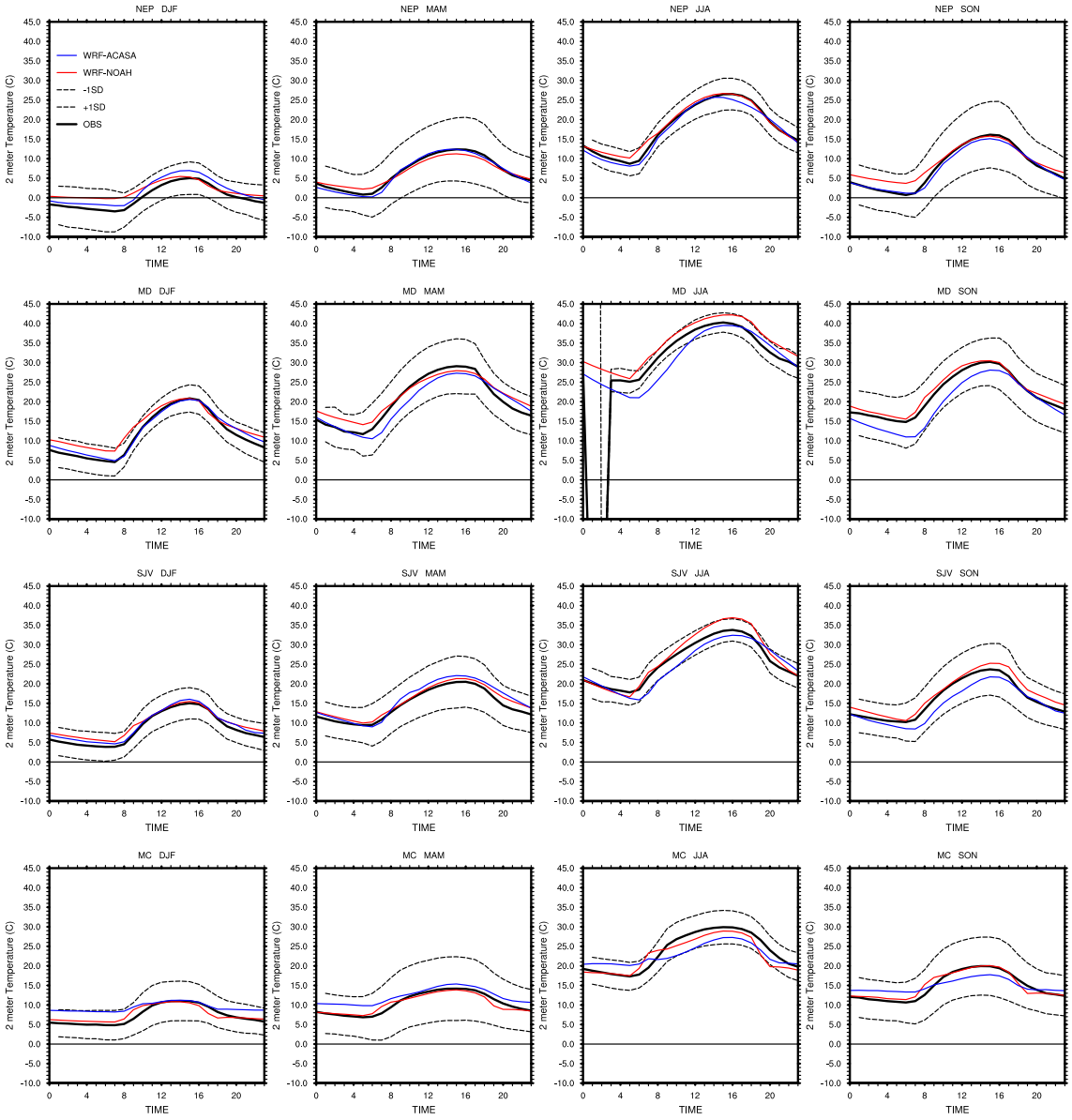

Figure 7. Diurnal cycle of surface air temperature for each season by station. The solid and the two dash black lines represent the surface observation and ± 1 standard deviation from the mean respectively. The WRF-ACASA results are in blue and the WRF-NOAH results are in red. Top to bottom: Northeast Plateau station, Mojave Desert station, San Joaquin Valley station, Mountain County station; Left to right: winter (DJF), spring (MAM), summer (JJA), fall (SON).

Further investigation into the temperature differences between the two models in time evolution and diurnal pattern reveals that these are results of differences in model representations of land cover type, as well as canopy structure of the two models. Both models agree most with the observation over the Northeast Plateau station. The site information indicated that this station is located over short vegetated grassland, which matches the land cover type assigned by the WRF model to that particular 8 km x 8 km grid-point. Even though the WRF-ACASA model uses a multilayer canopy representation for all its land cover types, there is no significant difference between the two models over this simple short grass canopy due to short canopy height. However, as the canopy becomes taller and more complex, the representations of canopy structure and plant physiology become more important. The correct representation of land cover is crucial. For example, the WRF model assigns a vegetation type of Evergreen Needleleaf Forest to the 8 km x 8 km grid point of the Mountain County station. However, a closer look at the MC station shows that the station is actually located at the edge of the forest, over a large clear-cut short grass area—not within the forest as assumed by the WRF-ACASA model, or above a single big leaf rough surface as assumed by the WRF-NOAH model. This mismatch of land cover type seems to be more problematic to the WRF-ACASA model than the WRF-NOAH model in its temperature simulations, probably because the single-leaf NOAH simulation is functionally similar to the actual conditions surrounding this site, unlike the complex forest understory simulated in ACASA.

While a single layer is used in the WRF-NOAH, the WRF-ACASA assumes a 17-meter canopy height with 10 vertical layers for this vegetation type. The surface air temperature simulated by the WRF-ACASA's multilayer canopy structure and radiation transfer scheme is calculated from within a canopy with overhead shading from tall trees, accounting for the microclimatic influences of understory temperature and humidity. Due to less direct heating from shortwave radiation, daytime temperatures within the canopy layers as simulated by WRF-ACASA during the warm months of May and August are respectively lower than the surface air temperature measured over a short grass area near the forest. In addition, the Needleleaf forest land cover type used in the WRF-ACASA model experiences turbulent transport and mixing of energy, moisture, gas, and momentum within the canopy layers resulting from the higher-order turbulent closure scheme. Therefore, unlike environmental conditions at the station at 2-meter height above the short grass area, the air at 2-meter height within the WRF-ACASA tall canopy experiences a drastic reduction in nighttime heat loss. Hence, the surface air temperatures of the WRF-ACASA simulation are higher than the surface observation during nighttime in February and November. Such details of canopy structures and their associated thermodynamic processes, however, are lacking from the single layer WRF-NOAH model, and do not match the observational site characteristics.

As mentioned before, the WRF-ACASA model tends to underpredict temperature observations during early summer morning in the Mojave Desert and the WRF-NOAH model tends to overpredict temperature all day. The prolonged cooling in the morning simulated by the WRF-ACASA model is associated with the low vegetated cover over shrublands. In this situation, more energy is lost from the surface to the atmosphere. In general, the model performances from

WRF-ACASA and WRF-NOAH vary depending on the season and the vegetation cover. The cool biases seen in desert regions may also be due to the nocturnal inversion issue described earlier.

Figure 8 shows scatter plots of simulated monthly surface air temperature from the WRF-ACASA and WRF-NOAH models versus observations, sorted by seasons for the four basins defined previously. Each of the points represents a monthly average for one station in the specified basin, and the colors indicate seasons. Least squares regression of the seasonal data shows that both model simulations approach a 1:1 line relationship with the observations. There are some small differences in performances between the two models depending on seasons and locations. This collective analysis of all stations from the four basins shows that although there are some cold biases over the Mojave Desert station, the models generally perform well across the entire basin.

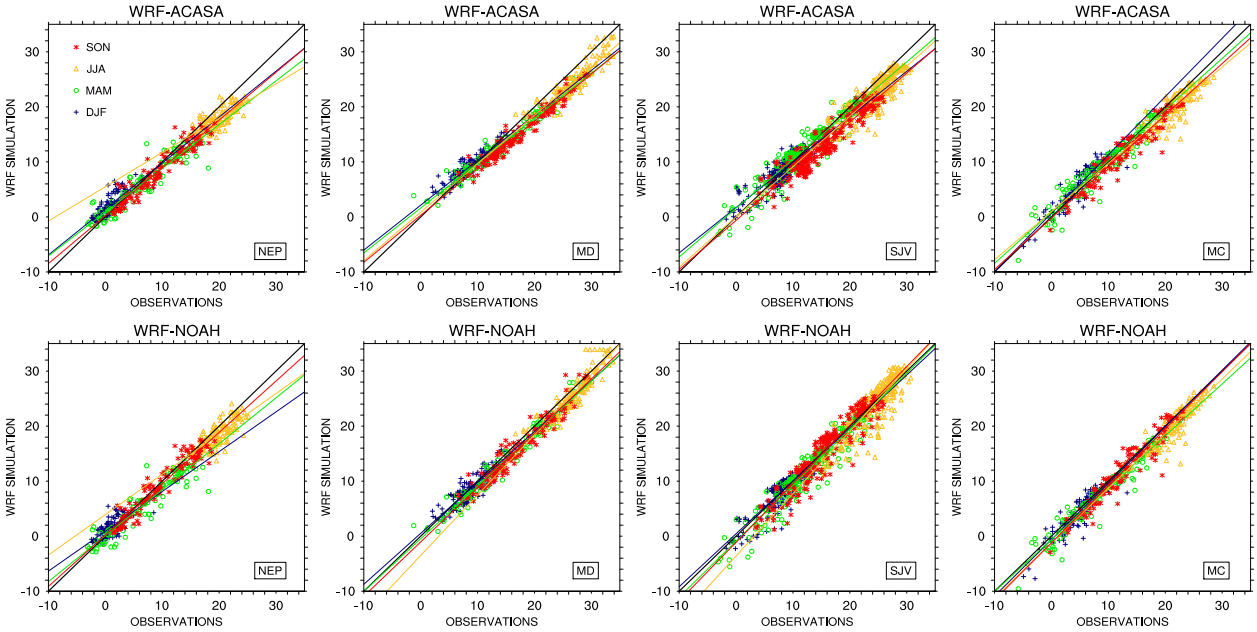

Figure 8. Scatter plots for monthly air temperature simulated by WRF-ACASA (top) and WRF-NOAH (bottom) for the 4 basins: (Left to right) Northeast Plateau station, Mojave Desert station, San Joaquin Valley station, Mountain County station. Each color simple represents different season: Blue cross = winter (DJF), Green circle = spring (MAM), Yellow triangle = summer (JJA), Red asterisk = fall (SON).

Table 2 and **Figure 9** present the statistical analysis of the WRF-ACASA and WRF-NOAH near-surface temperature outputs for each of California's 13 basins. Statistical values of R-square value, Root Mean Square Error (RMSE), and Degree of Agreement are calculated for each of the basin for each of four seasons. The Coefficient of Determination (or R-square) represents the correlation of the model simulation with the surface observation. The RMSE shows the relative errors of the model simulation against the observation, while the Degree of Agreement is a statistical method to assess the agreement between the model simulations with the surface observation.

Table 2. Selected sites from the Air Resources Board meteorological stations network.

		R^2		RMSE		Degree of Agreement	
Season	**Basin**	**WRF-NOAH**	**WRF-ACASA**	**WRF-NOAH**	**WRF-ACASA**	**WRF-NOAH**	**WRF-ACASA**
DJF	SCC	0.831671	0.716923	1.73878	2.46986	0.91687	0.821745
MAM	SCC	0.98397	0.806324	1.32221	2.09018	0.987497	0.910685
JJA	SCC	0.603668	0.532604	2.03934	2.2107	0.93101	0.899527
SON	SCC	0.817867	0.8446	1.79367	1.7037	0.934533	0.951894
DJF	SJV	0.996713	0.944033	1.49348	1.55048	0.996796	0.969605
MAM	SJV	0.989379	0.983285	1.81218	1.70317	0.991555	0.991714
JJA	SJV	0.981085	0.790353	2.24522	2.77545	0.97525	0.71053
SON	SJV	0.995999	0.836214	1.9562	2.83981	0.997329	0.88651
DJF	NCC	0.738797	0.624952	1.4336	2.15347	0.885708	0.703579
MAM	NCC	0.977027	0.804917	1.21572	1.65924	0.98831	0.952791
JJA	NCC	0.891338	0.796365	1.91748	1.78896	0.968166	0.947152
SON	NCC	0.945243	0.961512	1.53172	1.16758	0.96535	0.986446
DJF	SC	0.967272	0.913497	1.88247	1.64677	0.966178	0.948648
MAM	SC	0.993072	0.981621	1.55349	1.37131	0.993048	0.990378
JJA	SC	0.588722	0.580935	2.06404	3.4954	0.831568	0.595515
SON	SC	0.980249	0.710668	1.89105	2.40559	0.988638	0.831628
DJF	SV	0.986383	0.925806	1.1287	1.28074	0.991035	0.964948
MAM	SV	0.980696	0.981402	1.29392	1.21403	0.98801	0.992255
JJA	SV	0.99783	0.752783	1.64352	2.453	0.997999	0.67696
SON	SV	0.997573	0.881367	1.46927	2.09812	0.99837	0.919228
DJF	SD	0.951017	0.764242	1.46921	1.9857	0.96677	0.85756
MAM	SD	0.966413	0.926948	1.15405	1.26534	0.975935	0.973743
JJA	SD	0.487301	0.554737	2.05678	3.64936	0.768834	0.612857
SON	SD	0.875988	0.564617	1.47285	2.1236	0.946929	0.800983
DJF	GBV	0.813173	0.754106	2.7741	3.40534	0.952817	0.908663
MAM	GBV	0.93591	0.936978	2.36249	2.20798	0.962156	0.969805
JJA	GBV	0.853203	0.804406	2.64441	3.01706	0.856085	0.739935
SON	GBV	0.92474	0.917856	2.2518	2.34017	0.966767	0.963998
DJF	SFB	0.185791	0.284025	1.77587	2.0497	0.876986	0.886728
MAM	SFB	0.913346	0.63263	1.51517	2.0793	0.976113	0.941796
JJA	SFB	0.743593	0.495629	1.93917	3.10351	0.924286	0.768198
SON	SFB	0.950796	0.629486	1.4078	1.98632	0.981719	0.848947
DJF	SS	0.496889	0.727061	1.86463	2.19616	0.876449	0.901978
MAM	SS	0.994308	0.910398	1.2895	1.67741	0.996386	0.964686
JJA	SS	0.679887	0.391227	2.58393	2.63565	0.790626	0.684046
SON	SS	0.991819	0.769102	1.59417	3.04378	0.996416	0.865084
DJF	NEP	0.813234	0.762997	1.46407	1.81746	0.947417	0.897551
MAM	NEP	0.926788	0.928542	2.14003	1.96821	0.968855	0.976753
JJA	NEP	0.743007	0.59725	2.09303	2.52024	0.861164	0.769247
SON	NEP	0.987654	0.936724	1.54218	1.83687	0.99447	0.972525
DJF	MD	0.991988	0.904003	1.37581	1.27348	0.996475	0.971514
MAM	MD	0.969527	0.921582	1.62038	1.88437	0.982023	0.969443
JJA	MD	0.957873	0.74645	1.99593	2.84406	0.960473	0.72887
SON	MD	0.948833	0.824341	1.90569	2.55955	0.966272	0.884061
DJF	MC	0.983341	0.945083	1.61558	1.75623	0.982671	0.952361
MAM	MC	0.965586	0.991983	1.87782	1.76668	0.977757	0.996098
JJA	MC	0.898993	0.830306	2.1299	2.39603	0.893741	0.834615
SON	MC	0.982515	0.963089	1.81802	1.81886	0.987068	0.977584
DJF	NC	0.890632	0.751115	1.45055	1.89727	0.96326	0.919472
MAM	NC	0.677484	0.64897	3.47913	3.17359	0.872094	0.911504
JJA	NC	0.631845	0.631316	2.60202	2.92231	0.7467	0.629611
SON	NC	0.948986	0.876387	1.76809	1.87418	0.976128	0.951667

Figure 9. Statistical analysis of two model simulations versus observed for R-square, Root Mean Square Error (RMSE), and Degree of Agreement for the four different seasons. Basin: South Central Coast (SCC), San Joaquin Valley (SJV), North Central Coast (NCC), South Coast (SC), Sacramento Valley (SV), San Diego county(SD), Great Basin Valleys(GBV), San Francisco Bay(SFB), Salton Sea (SS), Northeast Plateau (NEP), Mojave Desert (MD), Mountain Counties (MC), North Coast (NC) Season: winter (DJF), spring (MAM), summer (JJA), fall (SON).

Overall, both of the models have a high degree of agreement with all 700 observation stations within the 13 ARB basins during winter, spring, and autumn. The dry summer season is more problematic than the other seasons for both of the models and more so for the WRF-ACASA model over coastal regions such as South Coast, San Diego, and San Francisco basins. This is most noticeable in the RMSE values for WRF-ACASA over the low vegetated regions of Great Basin Valley (GBV), Salton Sea (SS), and San Diego (SD), which increased dramatically during the warm season. While the Degree of Agreement for the San Francisco Basin (SFB) during the wintertime is high with values above 0.8 for both models, the R-square values show that there is little correlation between the model simulations and the surface observations. It could be due to the small range of observation data. Overall, the temperature simulations from both models agree well with the observations with a high Degree of Agreement. Previous examination on a station-by-station basis also reveals that there is a mismatch in vegetation cover between what is in the WRF models and the actual land surface at the station (e.g., the Mountain County station from Table 1). These mismatches introduce errors that are not due to model physics, and they contribute to some of the low R-square and high RMSE values in the collective study.

Figure 10 shows time series of surface dew point temperature over the same four stations (NEP, MD, SJV, MC). The dew point temperature influences land surface interaction with the atmosphere by indicating conditions for condensation. The disparities between the WRF-ACASA and WRF-NOAH models are more distinct in the dew point temperature than in the surface temperature: while both models perform well with the surface temperature simulation, the WRF-ACASA model outperforms the WRF-NOAH in simulating the dew point temperature, especially over the San Joaquin station and during May for the Mojave Desert station. This could be because the complex physiological processes in the WRF-ACASA model allow a more accurate simulation of the humidity profile and physiological interactions. Although the vegetation covers over these two regions are sparse, the multilayer canopy structure in the WRF-ACASA model is likely to retain moisture longer within the canopy. These details put the dew point temperature calculated by WRF-ACASA closer to observations than the WRF-NOAH model, which can only account for a single canopy layer.

Both models have difficulty over the Mojave Desert station, where they underestimated the dew point temperature as much as 15°C during February and November. Similar to the surface temperature analysis, both models performed best over the Northeast Plateau station with well-matched land cover type (WRF-ACASA) and simple canopy structure of short grass (WRF-NOAH). In general, the dew point temperature simulations from the WRF-ACASA model match closely with the observations in magnitude and timing.

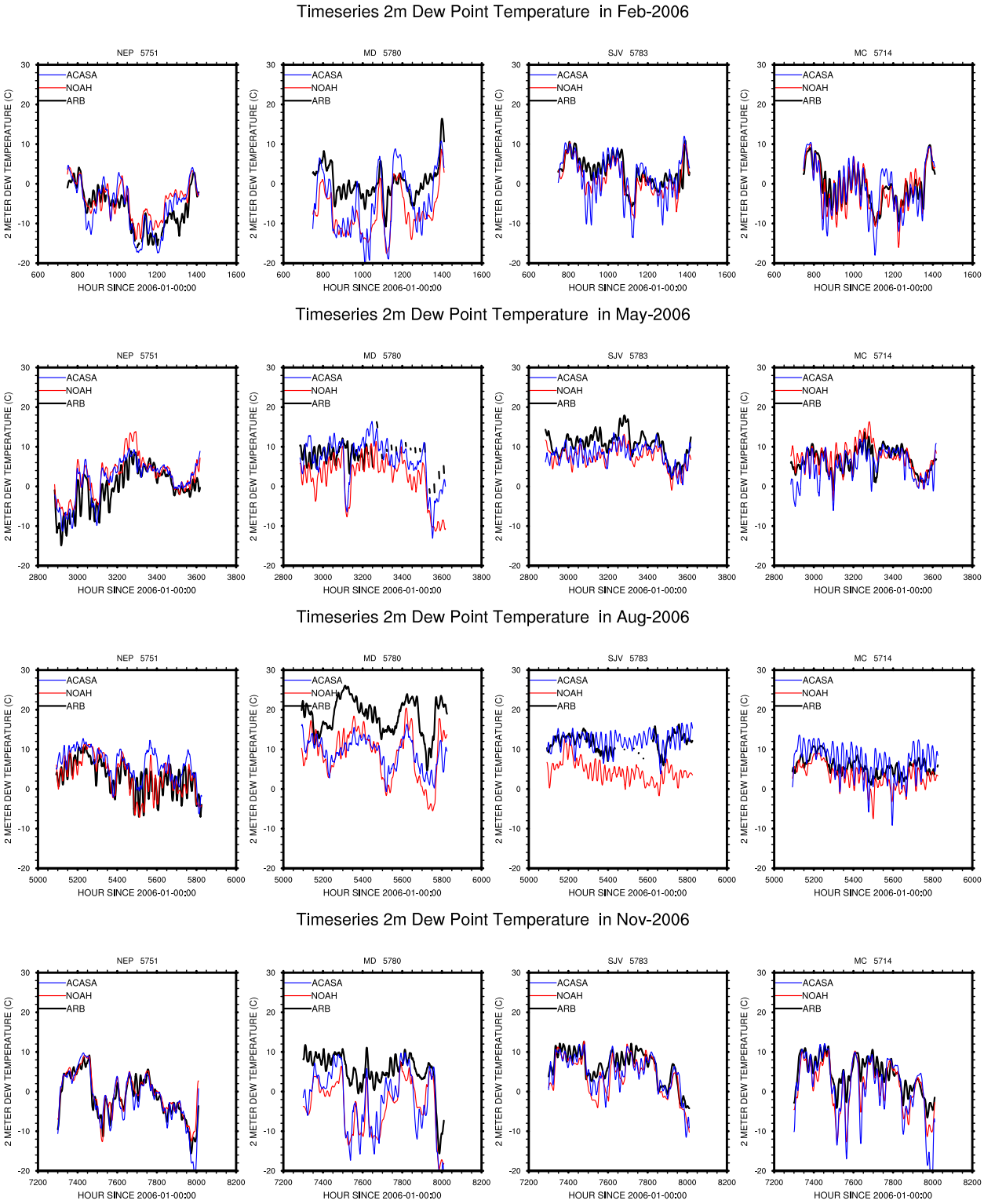

Figure 10. Time series of dew point model predictions and observations for four stations during February, May, August, and November 2006. Left to right: NEP, MD, SJV, MC.

Figure 11 presents diurnal patterns of surface dew point temperature for the four seasons. Unlike for the surface air temperature, there is relatively little diurnal variation in the surface dew point temperature throughout the seasons and locations. The simulated dew point temperatures in both WRF-ACASA and WRF-NOAH are functions of surface pressure and surface water vapor mixing ratio. Since the surface pressure does not change dramatically throughout the day, changes in dew point temperature are mainly due to fluctuations in water vapor mixing ratio. Once again, the dry arid and low vegetated Mojave Desert site is problematic for both models.

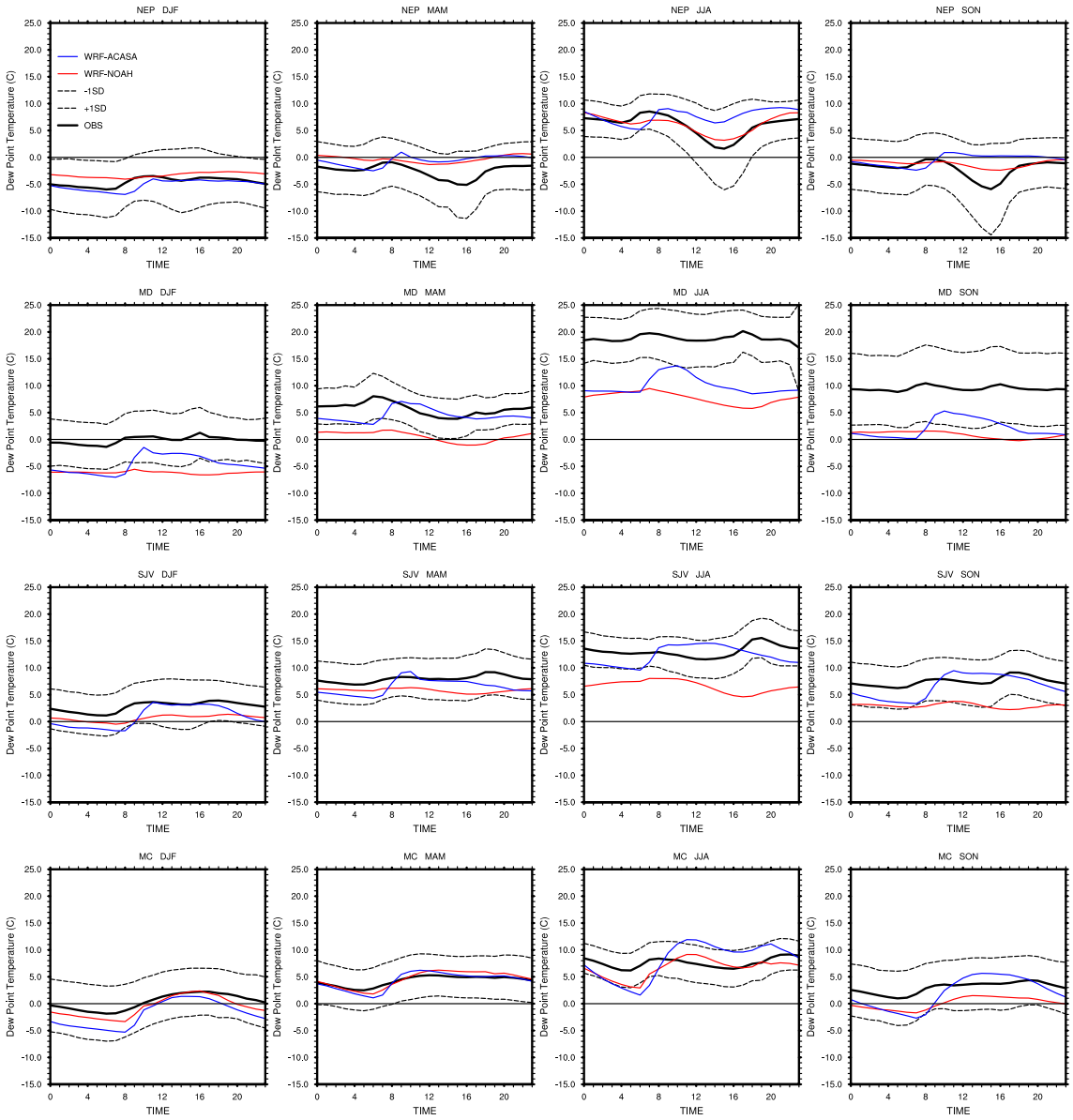

Figure 11. Mean diurnal dew point temperature trends for the four seasons and the four stations. Top to bottom: NEP, MD, SJV, MC. Left to right: winter (DJF) spring (MAM), summer (JJA), fall (SON).

Compared to the surface temperature, **Figure 12** shows that the model simulations on dew point temperature exhibit more scatter than for other observational sets examined thus far, although Figure 10 seems to indicate that WRF-ACASA has a better agreement with surface ob-

servations at the MD station. The seasonal patterns for the entire Mojave Desert Basin show that both WRF-ACASA and WRF-NOAH performances are comparatively poor in this sparsely vegetated region. The choice of land surface model did not affect the model simulation; hence, the problem could be in the atmospheric processes in WRF and not in the land surface processes.

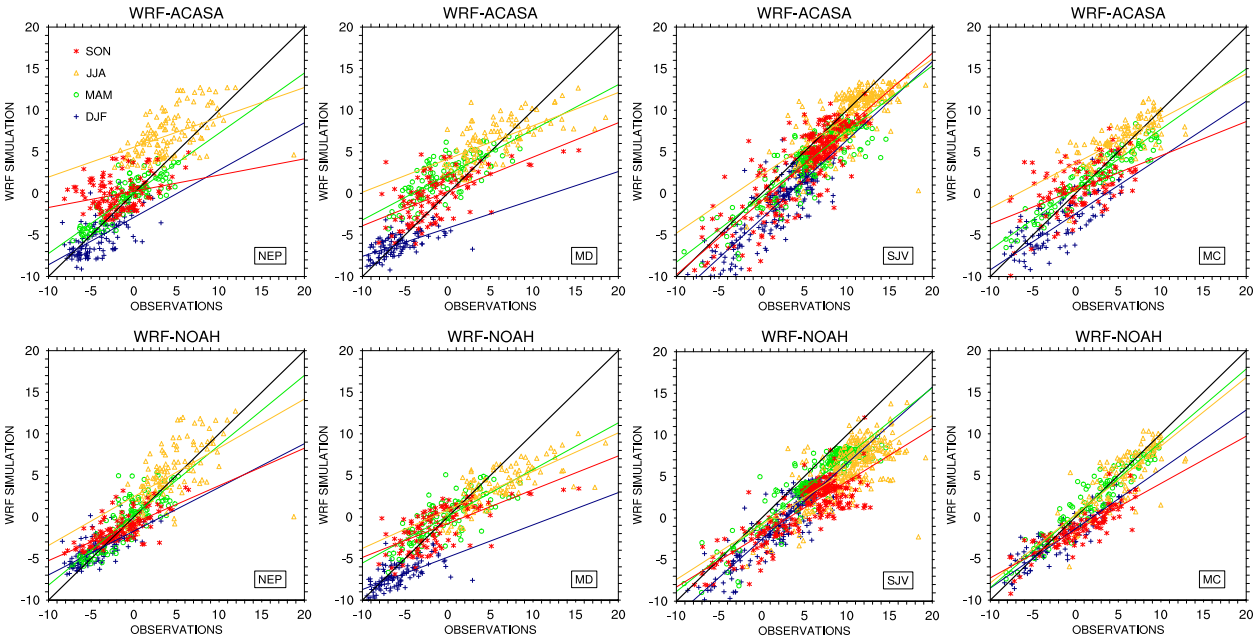

Figure 12. Time series of surface dew point temperature simulated by WRF-ACASA and WRF-NOAH, with surface observations for four different stations during the months of February, May, August and November 2006.

This could be the result of the assumption of horizontal homogeneity in each of the 8 km x 8 km grid cells used in both WRF-ACASA and WRF-NOAH. A single homogeneous grid cell could be representing several observation stations with different microclimatic conditions. This is especially important when, for example, the shrublands in the Mojave Desert Basin have different degrees of canopy openness. Unlike the previous analysis, Figure 12 shows that the WRF-ACASA model underperforms relative to WRF-NOAH over the Northeast Plateau basin.

Figure 13 compares the relative humidity from both WRF-ACASA and WRF-NOAH with the surface observation for four different locations during February, May, August and October of 2006. Except for the Mountain County station, both models fall mostly within the ± 1 standard deviation range with the WRF-ACASA model showing somewhat better agreement than the WRF-NOAH model over the Mojave Desert station. The WRF-NOAH model underestimates the relative humidity for Mojave Desert and San Joaquin Valley throughout the year. Although there is a land cover mismatch between the actual station and the model, the higher relative humidity values in the WRF-ACASA simulation compared with WRF-NOAH during the warm season reinforce that the multi-layer canopy structure and higher order turbulent closure scheme help the vegetation parameterization to simulate the retention of more moisture within the canopy layers.

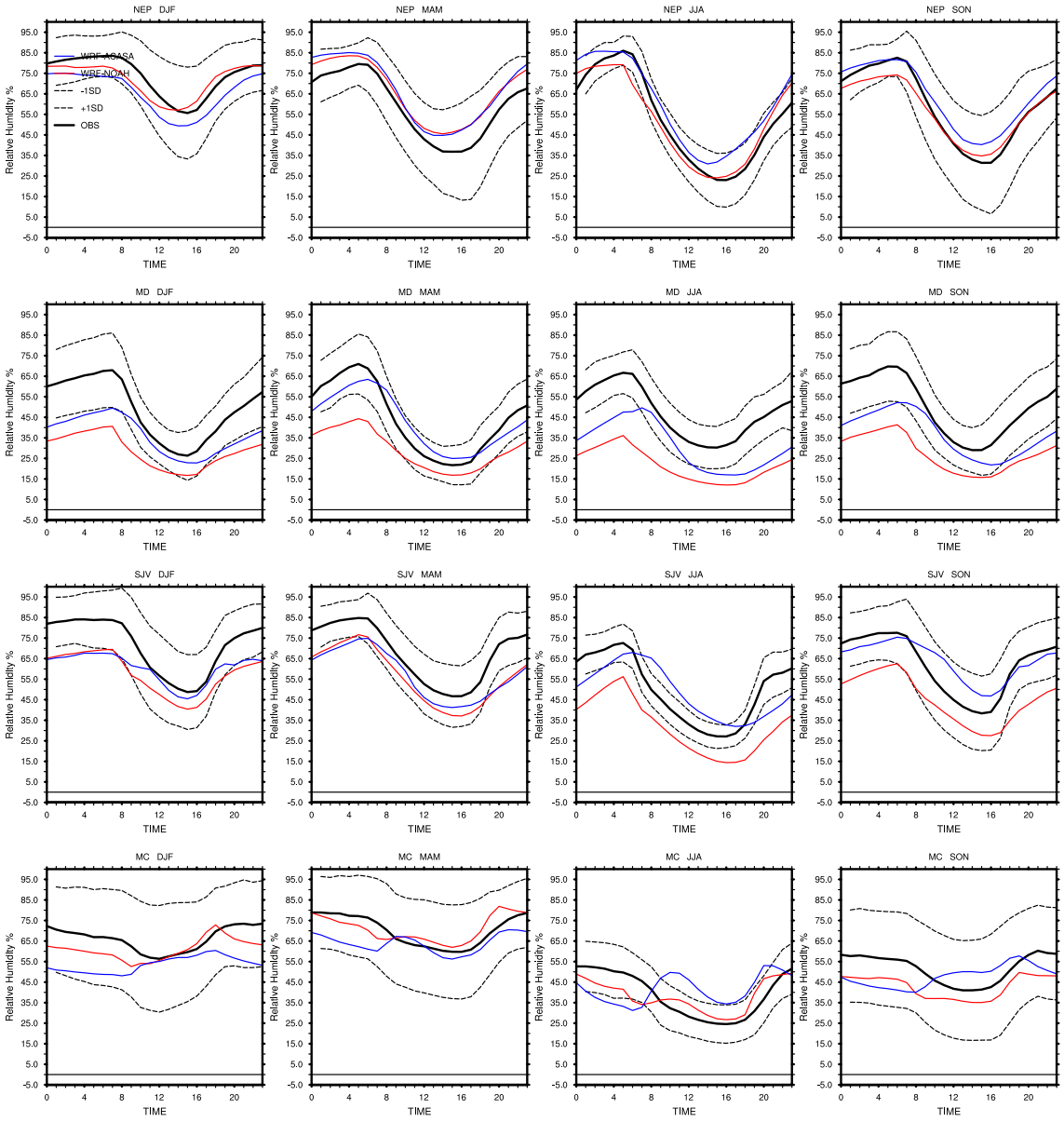

Figure 13. Time series of surface relative humidity simulated by WRF-ACASA and WRF-NOAH and the surface observations for four different stations during winter, spring, summer and fall of 2006.

The land cover mismatch in the model could lead to overestimation of the relative humidity in areas of low vegetation cover. The high LAI values over Central Valley and the assumption of horizontal homogeneity with one dominant vegetation cover cause the WRF-ACASA model to preserve too much water within the canopy layers during the warm August conditions instead of evaporating the water rapidly. As a result, WRF-ACASA overestimated the daytime relative humidity.

Figure 14 shows a Taylor diagram of monthly mean surface air temperature, dew point temperature, relative humidity, wind speed, and solar radiation simulated by WRF-ACASA and WRF-NOAH for all 730 stations in California. The Taylor diagrams for the four different seasons shows that simulations from both models agree well with the surface measurement in every

area except for wind speed. The surface air temperature, with high correlations, low RMSEs, and matching variability, is the most accurately simulated variable by both models when compared to the surface observations. While the WRF-NOAH model has a slightly better standard deviation for the air temperature, the WRF-ACASA is slightly more accurate for dew point temperature. Relative humidity, on the other hand, shows low correlation and high root mean square error from both models. These high root mean square errors and poor correlations could be attributed to the models' assumption of homogenous vegetation and leaf area cover for each grid cell, especially over low vegetated regions (as previously mentioned).

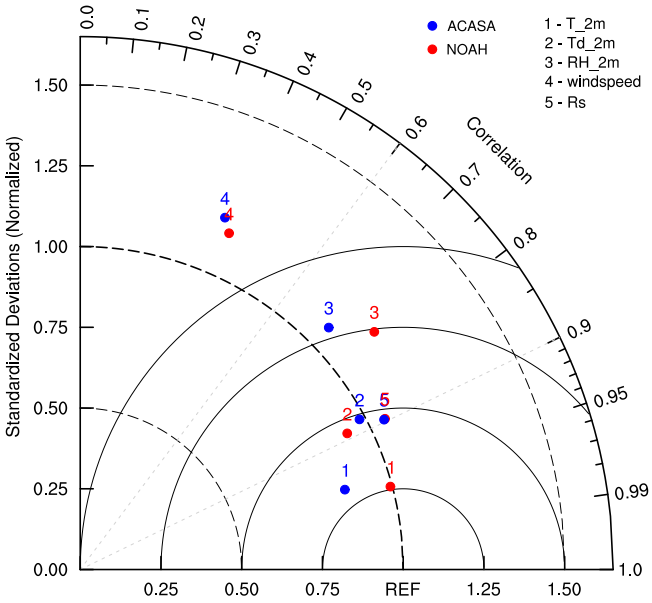

Figure 14. Taylor diagram of monthly mean surface air temperature, dew point temperature, relative humidity, wind speed, and solar radiation for both WRF-ACASA and WRF-NOAH for all ARB stations. WRF-ACASA is represented by blue dots and WRF-NOAH by red dots.

4. CONCLUSIONS

This study compares and evaluates the two different approaches and varying complexity of ACASA and NOAH land surface models embedded in the state-of-art mesoscale model WRF, as they simulate the surface conditions over California on a regional scale. With vast differences in land cover, ecological and climatological conditions, the complex terrain of California provides an ideal region to test and evaluate both models. Analysis of model simulations for 2006 from both WRF-ACASA and WRF-NOAH were compared with surface observations from hundreds of stations from the California Air Resources Board network. While both ACASA and NOAH land surface models use four soil layers for below-ground representation, the WRF-NOAH uses a single-layer "big leaf" to represent the surface layer for all land cover types. In all single-layer models such as NOAH, there is no interaction or mixing within the canopy regardless of the specified vegetation type. In contrast, the ACASA land surface model uses a multi-layer canopy structure that varies according to land cover type. The complex physically based model includes intricate surface processes such as canopy structure, turbulent transport and mixing within and above

the canopy and sublayers, and interactions between canopy elements and the atmosphere. Light and precipitation from the atmospheric layers above are intercepted, infiltrated, and reflected within the canopy layers. These along with other meteorological and environmental forcings are drivers of plant physiological responses. In addition, the higher order closure scheme in ACASA allows down- and counter-gradient transport of carbon dioxide, water vapor, heat, and momentum within and above the canopy layers, and interaction with the atmosphere. Through plant evapotranspiration, photosynthesis, respiration, and roughness length, the surface ecosystem transforms environmental conditions and influences the atmosphere processes above by modifying surface temperature, dew point temperature, and relative humidity. Compared to the WRF-NOAH, which has a simplified surface and ecosystem representation, the WRF-ACASA coupled model presents a detailed picture of the physical and physiological interactions between the land surface and the atmosphere. Compared to 2-meter near surface observations, WRF-ACASA output may be better suited to simulate understory microclimate, as WRF-NOAH's "big leaf" has no understory.

Comparisons between model simulations and surface observations show that the WRF-ACASA model is able to soundly simulate surface and atmospheric conditions. Its simulation of temperature, dew point temperature, and relative humidity agree well with the surface observations overall. While both WRF-ACASA and WRF-NOAH simulations agree with the surface observations, model performances vary among land surface representations, depending on surface and atmosphere conditions. During the cold and wet winter, both models have a high degree of agreement as well as high correlation with the surface observations, in terms of surface temperature, dew point temperature and relative humidity. However, as the season starts to warm up, a temperature bias for WRF-ACASA in certain regions becomes apparent. Maximum daytime temperatures in the WRF-ACASA simulations are systematically lower than the observed daily maximum over low vegetated regions such as the Mojave Desert. This temperature bias is likely due to discrepancy in LAI causing excessive evaporative cooling. For the shrubland vegetation with low leaf area index, the leaf area indices for each of the sub-canopy layers are further reduced. The higher order turbulent closure scheme more effectively reflects the energy transport away from the surface level to induce heat loss. These thermodynamical processes allow the WRF-ACASA model to describe the prolonged period of cooling in early mornings. As a result, the high daytime temperature is underestimated in the multi-layer model.

The analysis of dew point temperature and relative humidity shows that these more detailed physical processes in WRF-ACASA seem to improve the accuracy of dew point temperature and relative humidity simulations compared to the WRF-NOAH model. The process parameterizations appear to allow the retention of more moisture within the canopy layers as well as the distribution of moisture within and above the canopy. With more complex and detailed canopy and plant physiological process parameterizations, WRF-ACASA represents the ecosystem-atmosphere interactions more realistically than WRF-NOAH.

Overall, when compared to the simple single layer WRF-NOAH model, the WRF-ACASA model has greater model complexity, allowing it to present a more detailed picture of how the atmosphere and ecosystems interact–including ecophysiological activities such as photosynthesis and respiration–without decreasing the quality of the output. The physical and physiological

processes in WRF-ACASA highlight the effect of different land surface components and their overall impacts on atmospheric conditions. In addition, the WRF-ACASA model provides opportunities for more study on the topics of ecosystem responses to atmospheric impacts, such as the contribution of irrigation to canopy energy distribution, land use transformations, climate change, and other dynamic and biosphere-atmospheric atmosphere interactions.

Acknowledgements

This work is supported in part by the National Science Foundation under Awards No.ATM-0619139 and EF-1137306. The Joint Program on the Science and Policy of Global Change is funded by a number of federal agencies and a consortium of 40 industrial and foundation sponsors. (For the complete list see http://globalchange.mit.edu/sponsors/current.html). We also thank Dr. Matthias Falk for his inputs on the WRF-ACASA work.

5. REFERENCES

Borge, R., V. Alexandrov, J. José del Vas, J. Lumbreras and E. Rodríguez, 2008: A comprehensive sensitivity analysis of the WRF model for air quality applications over the Iberian Peninsula. *Atmos. Environ.*, **42**(37): 8560–8574.

Chen, F. and R. Avissar, 1994: The impact of land-surface wetness heterogeneity on mesoscale heat fluxes. *J. Appl. Meteor.*, **33**(11): 1323–1340.

Chen, F. and J. Dudhia, 2001a: Coupling an advanced land surface-hydrology model with the Penn State-NCAR MM5 modeling system. Part I: Model implementation and sensitivity. *Mon. Wea. Rev.*, **129**(4): 569–585.

Chen, F. and J. Dudhia, 2001b: Coupling an advanced land surface-hydrology model with the Penn State-NCAR MM5 modeling system. Part II: Preliminary model validation. *Mon. Wea. Rev.*, **129**(4): 587–604.

Chen, S. and J. Dudhia, 2000: Annual report: WRF physics. *Air Force Weather Agency*.

Chen, S. and W. Sun, 2002: A one-dimensional time dependent cloud model. *J. Meteor. Soc. Japan*, **80**(1): 99–118.

de Wit, M., 1999: Modelling nutrient fluxes from source to river load: a macroscopic analysis applied to the Rhine and Elbe basins. *Hydrobiologia*, **410**: 123–130.

Denmead, O. and E. Bradley, 1985: Flux-gradient relationships in a forest canopy. *The forest-atmosphere interaction: proceedings of the forest environmental measurements conference*, pp. 421–442.

Dickinson, R., A. Henderson-Sellers and P. Kennedy, 1993: Biosphere-Atmosphere Transfer Scheme (BATS) Version 1e as coupled to the NCAR community model. *NCAR Tech. Note NCAR/TN-387+ STR*, **72**.

Duan, Q., S. Sorooshian and V. Gupta, 1992: Effective and efficient global optimization for conceptual rainfall-runoff models. *Water Resour. Res.*, **28**(4): 1015–1031.

Dudhia, J., 1989: Numerical study of convection observed during the winter monsoon experiment using a mesoscale two-dimensional model. *J. Atmos. Sci.*, **46**(20): 3077–3107.

Etchevers, P., E. Martin, R. Brown, C. Fierz, Y. Lejeune, E. Bazile, A. Boone, Y. Dai, R. Essery, A. Fernandez *et al.*, 2004: Validation of the energy budget of an alpine snowpack simulated by several snow models (SnowMIP project). *Ann. Glaciol.*, **38**(1): 150–158.

Gao, W., R. Shaw and K. Paw U, 1989: Observation of organized structure in turbulent flow within and above a forest canopy. *Bound.Lay. Meteorol.*, **47**(1): 349–377.

Holtslag, A. and M. Ek, 1996: Simulation of surface flux and boundary layer development over the pine forest in HAPEX-MOBILHY. *J. Appl. Meteor.*, **35**(2).

Hong, S. and H. Pan, 1996: Nonlocal boundary layer vertical diffusion in a medium-range forecast model. *Mon. Wea. Rev.*, **124**(10): 2322–2339.

Houborg, R. and H. Soegaard, 2004: Regional simulation of ecosystem CO_2 and water vapor exchange for agricultural land using NOAA AVHRR and Terra MODIS satellite data. Application to Zealand, Denmark. *Remote Sens. Environ.*, **93**(1): 150–167.

Jarvis, P., 1976: The interpretation of the variations in leaf water potential and stomatal conductance found in canopies in the field. *Philos. Trans. Roy. Soc. London A*, **273**(927): 593–610.

Jetten, V., A. de Roo and D. Favis-Mortlock, 1999: Evaluation of field-scale and catchment-scale soil erosion models. *Catena*, **37**(3): 521–541.

Mahrt, L. and M. Ek, 1984: The influence of atmospheric stability on potential evaporation. *Collections*.

Marras, S., D. Spano, C. Sirca, P. Duce, R. Snyder, R. Pyles and K. Paw U, 2008: Advanced-Canopy-Atmosphere-Soil Algorithm (ACASA model) for estimating mass and energy fluxes. *Ital. J. Agron.*, **3**(3 Suppl.): 793–794.

Marras, S., R. Pyles, C. Sirca, K. Paw U, R. Snyder, P. Duce and D. Spano, 2011: Evaluation of the Advanced Canopy–Atmosphere–Soil Algorithm (ACASA) model performance over Mediterranean maquis ecosystem. *Agric. For. Meteor.*, **151**(6): 730–745.

Meyers, T. and K. Paw U, 1986: Testing of a Higher-Order Closure Model for Modeling Airflow within and above Plant Canopies. *Bound.Lay. Meteorol.*, **37**: 297–311.

Meyers, T. and K. Paw U, 1987: Modelling the plant canopy micrometeorology with higher-order closure principles. *Agric. For. Meteor.*, **41**(1): 143–163.

Miglietta, M. and R. Rotunno, 2005: Simulations of moist nearly neutral flow over a ridge. *J. Atmos. Sci.*, **62**(5): 1410–1427.

Mintz, Y., 1981: A brief review of the present status of global precipitation estimates. *Report of the Workshop on Precipitation Measurements from Space*.

Mlawer, E., S. Taubman, P. Brown, M. Iacono and S. Clough, 1997: Radiative transfer for inhomogeneous atmospheres: RRTM, a validated correlated-k model for the longwave. *J. Geophys. Res.*, **102**(D14): 16663–16.

Noilhan, J. and S. Planton, 1989: A simple parameterization of land surface processes for meteorological models. *Mon. Wea. Rev.*, **117**(3): 536–549.

Perrin, C., C. Michel and V. Andréassian, 2001: Does a large number of parameters enhance model performance? Comparative assessment of common catchment model structures on 429 catchments. *J. Hydrol.*, **242**(3): 275–301.

Pielke, R., G. Marland, R. Betts, T. Chase, J. Eastman, J. Niles, S. Running *et al.*, 2002: The influence of land-use change and landscape dynamics on the climate system: relevance to climate-change policy beyond the radiative effect of greenhouse gases. *Philos. Trans. Roy. Soc. London A*, **360**(1797): 1705–1719.

Pleim, J. and A. Xiu, 1995: Development and testing of a surface flux and planetary boundary layer model for application in mesoscale models. *J. Appl. Meteor.*, **34**(1): 16–32.

Powers, J., 2007: Numerical prediction of an Antarctic severe wind event with the Weather Research and Forecasting (WRF) model. *Mon. Wea. Rev.*, **135**(9): 3134–3157.

Pyles, R., B. Weare and K. Paw U, 2000: The UCD Advanced Canopy-Atmosphere-Soil Algorithm: comparisons with observations from different climate and vegetation regimes. *Quart. J. Roy. Meteor. Soc.*, **126**: 2951–2980.

Pyles, R., B. Weare, K. Paw U and W. Gustafson, 2003: Coupling between the University of California, Davis, Advanced Canopy-Atmosphere-Soil Algorithm (ACASA) and MM5: Preliminary results for July 1998 for western North America. *J. Appl. Meteor.*, **42**(5): 557–569.

Pyles, R., K. Paw U and M. Falk, 2004: Directional wind shear within an old-growth temperate rainforest: observations and model results. *Agric. For. Meteor.*, **125**(1): 19–31.

Raupach, M. and J. Finnigan, 1988: 'Single-layer models of evaporation from plant canopies are incorrect but useful, whereas multilayer models are correct but useless': Discuss. *Aust. J. Plant Physiol.*, **15**(6): 705–716.

Rowntree, P., 1991: Atmospheric parameterization schemes for evaporation over land: Basic concepts and climate modeling aspects. In: *Land Surface Evaporation: Measurement and Parameterization*, T. Schmugge and J.-C. André, (eds.), Springer-Verlag: New York, pp. 5–29.

Rutter, N., R. Essery, J. Pomeroy, N. Altimir, K. Andreadis, I. Baker, A. Barr, P. Bartlett, A. Boone, H. Deng *et al.*, 2009: Evaluation of forest snow processes models (SnowMIP2). *J. Geophys. Res.*, **114**(D6): D06111.

Sellers, P., C. Tucker, G. Collatz, S. Los, C. Justice, D. Dazlich and D. Randall, 1996: A revised land surface parameterization (SiB2) for atmospheric GCMs. Part II: The generation of global fields of terrestrial biophysical parameters from satellite data. *J. Climate*, **9**(4): 706–737.

Smirnova, T., J. Brown and S. Benjamin, 1997: Performance of different soil model configurations in simulating ground surface temperature and surface fluxes. *Mon. Wea. Rev.*, **125**(8): 1870–1884.

Smirnova, T., J. Brown, S. Benjamin and D. Kim, 2000: Parameterization of cold-season processes in the MAPS. *J. Geophys. Res.*, **105**(D3): 4077–4086.

Staudt, K., A. Serafimovich, L. Siebicke, R. Pyles and E. Falge, 2011: Vertical structure of evapotranspiration at a forest site (a case study). *Agric. For. Meteor.*, **151**(6): 709–729.

Stauffer, D. and N. Seaman, 1990: Use of four-dimensional data assimilation in a limited-area mesoscale model. Part I: Experiments with synoptic-scale data. *Mon. Wea. Rev.*, **118**(6): 1250–1277.

Stauffer, D., N. Seaman and F. Binkowski, 1991: Use of four-dimensional data assimilation in a limited-area mesoscale model. II- Effects of data assimilation within the planetary boundary layer. *Mon. Wea. Rev.*, **119**: 734–754.

Stull, R. B., 1988: *An introduction to boundary layer meteorology*. Kluwer Academic Publishers.

Su, H., K. Paw U and R. Shaw, 1996: Development of a coupled leaf and canopy model for the simulation of plant-atmosphere interactions. *J. Appl. Meteor.*, **35**: 733–748.

Thompson, S., B. Govindasamy, A. Mirin, K. Caldeira, C. Delire, J. Milovich, M. Wickett and D. Erickson, 2004: Quantifying the effects of CO_2-fertilized vegetation on future global climate and carbon dynamics. *Geophys. Res. Lett.*, **31**(23): L23211.

Trenberth, K. and D. Shea, 2006: Atlantic hurricanes and natural variability in 2005. *Geophys. Res. Lett.*, **33**(12): L12704.

Wieringa, J., 1986: Roughness-dependent geographical interpolation of surface wind speed averages. *Quart. J. Roy. Meteor. Soc.*, **112**(473): 867–889.

Xiu, A. and J. Pleim, 2001: Development of a land surface model. Part I: Application in a mesoscale meteorological model. *J. Appl. Meteor.*, **40**(2): 192–209.

Zhan, X. and W. Kustas, 2001: A coupled model of land surface CO_2 and energy fluxes using remote sensing data. *Agric. For. Meteor.*, **107**(2): 131–152.

Zhao, M., A. Pitman and T. Chase, 2001: The impact of land cover change on the atmospheric circulation. *Clim. Dyn.*, **17**(5): 467–477.

REPORT SERIES of the MIT Joint Program on the Science and Policy of Global Change

FOR THE COMPLETE LIST OF JOINT PROGRAM REPORTS: http://globalchange.mit.edu/pubs/all-reports.php

224. Cap-and-Trade Climate Policies with Price-Regulated Industries: *How Costly are Free Allowances?* *Lanz and Rausch* July 2012

225. Distributional and Efficiency Impacts of Clean and Renewable Energy Standards for Electricity *Rausch and Mowers* July 2012

226. The Economic, Energy, and GHG Emissions Impacts of Proposed 2017–2025 Vehicle Fuel Economy Standards in the United States *Karplus and Paltsev* July 2012

227. Impacts of Land-Use and Biofuels Policy on Climate: *Temperature and Localized Impacts* *Hallgren et al.* August 2012

228. Carbon Tax Revenue and the Budget Deficit: *A Win-Win-Win Solution?* *Sebastian Rausch and John Reilly* August 2012

229. CLM-AG: An Agriculture Module for the Community Land Model version 3.5 *Gueneau et al.* September 2012

230. Quantifying Regional Economic Impacts of CO_2 Intensity Targets in China *Zhang et al.* September 2012

231. The Future Energy and GHG Emissions Impact of Alternative Personal Transportation Pathways in China *Kishimoto et al.* September 2012

232. Will Economic Restructuring in China Reduce Trade Embodied CO_2 Emissions? *Qi et al.* October 2012

233. Climate Co-benefits of Tighter SO_2 and NO_x Regulations in China *Nam et al.* October 2012

234. Shale Gas Production: *Potential versus Actual GHG Emissions* *O'Sullivan and Paltsev* November 2012

235. Non-Nuclear, Low-Carbon, or Both? *The Case of Taiwan* *Chen* December 2012

236. Modeling Water Resource Systems under Climate Change: *IGSM-WRS* *Strzepek et al.* December 2012

237. Analyzing the Regional Impact of a Fossil Energy Cap in China *Zhang et al.* January 2013

238. Market Cost of Renewable Jet Fuel Adoption in the United States *Winchester et al.* January 2013

239. Analysis of U.S. Water Resources under Climate Change *Blanc et al.* February 2013

240. Protection of Coastal Infrastructure under Rising Flood Risk *Lickley et al.* March 2013

241. Consumption-Based Adjustment of China's Emissions-Intensity Targets: *An Analysis of its Potential Economic Effects* *Springmann et al.* March 2013

242. The Energy and CO_2 Emissions Impact of Renewable Energy Development in China *Zhang et al.* April 2013

243. Integrated Economic and Climate Projections for Impact Assessment *Paltsev et al.* May 2013

244. A Framework for Modeling Uncertainty in Regional Climate Change *Monier et al.* May 2013

245. Climate Change Impacts on Extreme Events in the United States: An Uncertainty Analysis *Monier and Gao* May 2013

246. Probabilistic Projections of 21st Century Climate Change over Northern Eurasia *Monier et al.* July 2013

247. What GHG Concentration Targets are Reachable in this Century? *Paltsev et al.* July 2013

248. The Energy and Economic Impacts of Expanding International Emissions Trading *Qi et al.* August 2013

249. Limited Sectoral Trading between the EU ETS and China *Gavard et al.* August 2013

250. The Association of Large-Scale Climate Variability and Teleconnections on Wind Resource over Europe and its Intermittency *Kriesche and Schlosser* September 2013

251. Regulatory Control of Vehicle and Power Plant Emissions: *How Effective and at What Cost?* *Paltsev et al.* October 2013

252. Synergy between Pollution and Carbon Emissions Control: *Comparing China and the U.S.* *Nam et al.* October 2013

253. An Analogue Approach to Identify Extreme Precipitation Events: *Evaluation and Application to CMIP5 Climate Models in the United States* *Gao et al.* November 2013

254. The Future of Global Water Stress: *An Integrated Assessment* *Schlosser et al.* January 2014

255. The Mercury Game: *Evaluating a Negotiation Simulation that Teaches Students about Science–Policy Interactions* *Stokes and Selin* January 2014

256. The Potential Wind Power Resource in Australia: *A New Perspective* *Hallgren et al.* February 2014

257. Equity and Emissions Trading in China *Zhang et al.* February 2014

258. Characterization of the Wind Power Resource in Europe and its Intermittency *Cosseron et al.* March 2014

259. A Self-Consistent Method to Assess Air Quality Co-Benefits from US Climate Policies *Saari et al.* April 2014

260. Electricity Generation and Emissions Reduction Decisions under Policy Uncertainty: *A General Equilibrium Analysis* *Morris et al.* April 2014

261. An Integrated Assessment of China's Wind Energy Potential *Zhang et al.* April 2014

262. The China-in-Global Energy Model *Qi et al.* May 2014

263. Markets versus Regulation: *The Efficiency and Distributional Impacts of U.S. Climate Policy Proposals* *Rausch and Karplus* May 2014

264. Expectations for a New Climate Agreement *Henry D. Jacoby and Y.-H. Henry Chen* August 2014

265. Coupling the High Complexity Land Surface Model ACASA to the Mesoscale Model WRF *Xu et al.* August 2014

Contact the Joint Program Office to request a copy. The Report Series is distributed at no charge.